ChemComm

Accepted Manuscript

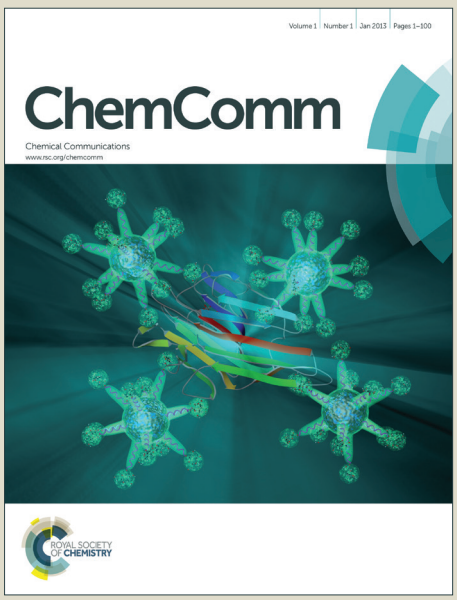

ROYAL SOCIETY OF CHEMISTRY

www.rsc.org/chemcomm

Cite this: DOI: 10.1039/c0xx00000x
www.rsc.org/xxxxxx

ARTICLE TYPE

X-ray Chemical Imaging and Electronic Structure of a Single Nanoplatelet Ni/Graphene Composite

Chunyu Zhou[a], Jian Wang[b]*, and Jerzy A. Szpunar[a]*

Received (in XXX, XXX) Xth XXXXXXXXX 20XX, Accepted Xth XXXXXXXXX 20XX
DOI: 10.1039/b000000x

Chemical imaging and quantitative analysis of a single graphene nanoplatelet grown with Ni nanoparticles (Ni/Graphene) has been performed by scanning transmission X-ray microscopy (STXM). Local electronic and chemical structure of Ni/Graphene has been investigated by spatially resolved C, O K-edges and Ni L-edge X-ray absorption using near edge structure (XANES) spectroscopy, revealing the covalent anchoring of Ni(0) on graphene. This study facilitates understanding of the structure modification of host material for hydrogen storage and offers a better understanding of interaction between Ni particles and graphene.

Growing demands for sustainable and clean energy are a huge challenge for the world economy as conventional energy sources are being steadily depleted [1, 2]. Among various energy sources, hydrogen is becoming attractive due to its lightweight, and environmentally friendly features[1, 3, 4]. The development of this alternative energy source for future economy requires not only inexpensive production of hydrogen, but also the safety and efficiency of storage and delivery for practical applications. Hydrogen storage has been commonly studied in the forms of compressed gas[5], liquid hydrogen[6], condensed state[7]. However, if one is concerned with the weight, safety, environmental protection, durability and cost efficiency, the optimum choice would be some solid state materials[8] in compact form. Various nanostructured materials have been considered for this application. Graphene recently emerges as a promising hydrogen storage medium with attractive features, such as low weight, high chemical stability and extremely high specific surface area (up to 2600 cm^2/g)[9, 10]. Nevertheless, as a non-polar molecule, hydrogen is very weakly bounded to prinstine graphene via van der Waals's forces[11, 12], which result in a low hydrogen sorption. Although metal catalyst or metallic compounds are active materials and have strong interactions with hydrogen via chemical bonds[13], the bare metal particles easily aggregate to clusters [14] providing insufficient "anchoring sites", leading to a chemically inert system for gaseous hydrogen uptake. To overcome these drawbacks, doping metal particles, especially transition metal (TM) on graphene should significantly strengthen the interaction among hydrogen, metal and graphene[8, 11, 14-16], i.e. TM particles, if uniformly dispersed on the surface of graphene, can serve as spacers of layered graphene structure and are hydrogen receptors, thus they further promote a dissociative chemisorption via hydrogen spillover process[17]. This surface modification of graphene by TM nanoparticles should greatly enhance hydrogen capacity for storage and discharge because of both physisorption in pristine graphene and chemisorption in metal. Among the TMs, the presence of Ni not only alters the geometry of graphene network, resulting in enhanced structure stability[18-21] of the hydrogen host material, but also actively serves as dissociative sites for hydrogen chemisorption[22-24]. So far detailed analysis of the mechanism of TM/graphene interaction is still missing. A combination of X-ray absorption near edge structure (XANES) spectroscopy and scanning transmission X-ray microscopy (STXM) has been widely applied to investigate the chemical interaction and speciation in pristine graphene[25] and various graphene-based hybrid nanostructures. Problems like layered structure in r-GO[25], dopant distribution in N-CNT[26], state of charge (SOC) in $LiMn_xFe_{1-x}PO4$/graphene[27] as well as interaction within nanostructures consisting of graphene and metallic compounds or alloy hybrids[26-29] have already been investigated. This work reports STXM characterization of Ni/Graphene as a potential hydrogen storage medium. Specifically, chemical imaging and component identification was performed on a single Ni/Graphene nanoplatelet. Furthermore, spatially resolved XANES spectroscopy was obtained at the C, O K-edges and Ni L-edge to investigate the local chemistry and electronic structure, particularly Ni valence state and chemical interactions involved in Ni/Graphene. TM/graphene has been synthesized through thermal reduction[24, 30-32], CVD approach[20, 21, 33, 34] and so forth, yet the scalability and cost efficiency of synthesis still remain challenging. Here, we produced Ni/Graphene in a simple and scalable way by pressurized multiplex solvothermal reduction[35] and followed by thermal processing. The preparation details and laboratory-based characterizations are briefly described in the supplementary information. STXM with spatial resolution of 30 nm was performed on the soft X-ray spectromicroscopy beamline 10ID-1 at the Canadian Light Source (CLS). XANES at the C, O K-edges and Ni L-edge were extracted from STXM image stacks scanned over a range of photon energies. For more details of

STXM experimental and data analysis, refer to other publications by the author[26, 27, 29, 36].

A high resolution STXM transmission (absorption) image at the Ni L_3-edge (853.3 eV) of a randomly selected Ni/Graphene nanoplatelet is shown in Fig. 1a. Ni particles can be clearly seen on the graphene nanoplatelet as dark spots and patches, which is consistent with the XRD results (Fig. S2 ESI) and SEM observations (Fig. S3 ESI), confirming the growth of Ni on graphene substrate in the nanostructured composite. Even with some degree of Ni aggregation, Fig. 1a still shows the majority of Ni particles on the graphene nanoplatelet are nanoscaled/sub-micron scaled size, and they are more widely and evenly distributed than the localized aggregation. Then medium resolution STXM image stacks were acquired on the same nanoplatelet at C, O K-edges and Ni L-edge in order to derive quantitative chemical maps of the components. Fig. 1b and 1c present the thickness map of graphene and Ni respectively, derived by fitting the C 1s and Ni 2p STXM stacks with the quantitatively scaled reference spectra of pure graphene and Ni. Fig. 1d displays the colour composite map of the Ni/Graphene nanoplatelet. The graphene thickness map shows the lateral size and thickness of the layered graphene from thermally reduction as ~10 μm and ~25 nm, respectively. In addition, thickness variation of Ni particles (up to 75 nm due to partially aggregation) displayed in Fig. 1c suggests that a high loading of Ni on graphene was successfully achieved. Interestingly, few aggregated Ni particles attached to the edge of the graphene nanoplatelet without support were also observed, probably due to particle migration during high temperature thermal processing or coordination of Ni particles to the dangling bonds within the edge

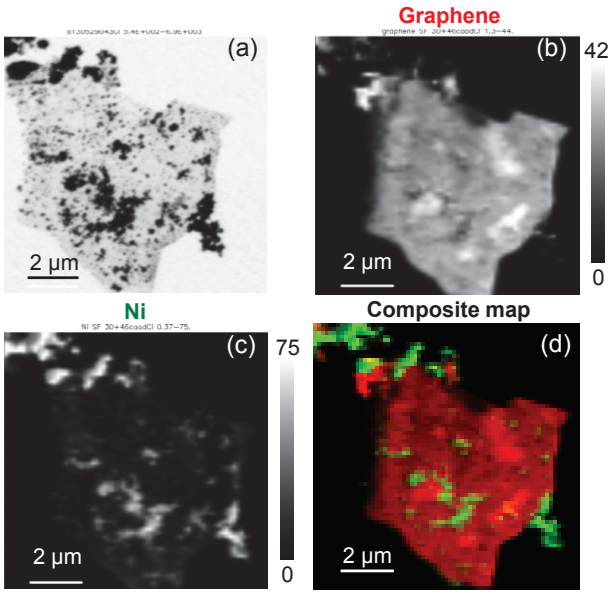

Fig. 1 STXM chemical imaging of a single Ni/Graphene nanoplatelet, (a) high resolution STXM transmission (absorption) image at the Ni L_3-edge (853.3 eV), in which the morphology of the metallic Ni particles and the substrate graphene nanoplatelet are clearly resolved; (b) Graphene and (c) Ni thickness maps derived by medium resolution STXM image stack scans, all vertical grey scales represent the materials thickness in nm, (d) colour composite map, red: graphene, green: Ni.

structure[18, 37, 38].

To further investigate the local chemistry and electronic structure of the composite, selected regions on the sample were used to extract XANES absolute absorbance (i.e. optical density) spectra from STXM stacks at the C, O K-edges and Ni L-edge in Fig. 2. These carefully selected regions as displayed in Fig. 2a include almost pure graphene (red regions), pure Ni particles off the nanoplatelet (green regions), and Ni/Graphene (blue regions). The extracted C K-edge XANES spectra from the selected regions in Fig. 2b confirm that the green spectrum is barely featured with carbon, i.e. unsupported Ni appears along or off the edge of graphene nanoplatelet, which is in good agreement with the chemical imaging in Fig. 1. However, the main peaks of Ni/Graphene (blue spectrum) are located at the same positions as those of almost pure graphene (red spectrum). To make a more quantitative analysis, a linear combination of the pure Ni and graphene spectra (i.e. 0.45*Ni + 1.0*Graphene, orange lines in Fig. 2) matching the pre- and post-edges of Ni/Graphene is included for comparison. This linear combination fit removes the sample thickness and other experimental effects, and serves as a reference spectrum to quantitatively compare Ni/Graphene and pure Ni + Graphene. Since XANES spectrum probes the projected unoccupied density of states (UDOS) near each emelmental edge, the spectral difference between Ni/Graphene and pure Ni + Graphene clearly shows the electronic structure change and subtle chemical composition difference between them. In general, XANES peak position is sensitive to the chemical envrionment of the X-ray absorbing atoms, such as functional group, oxidation state/valence, bonding type etc., while XANES peak intensity is propotional to the amount of the absorbing atoms, and related to the bonding orientation or chemical interactions between the absorbing atoms and the surrounding atoms, such as charge transfer, π-π interaction etc. It is commonly known that the spectral features at ~285 eV and ~292 eV are corresponding to the transitions from C 1s to graphitic states of π* and σ* respectively[25, 27]. These features confirm the preservation of graphitic framework in Ni/Graphene. The much stronger and broader π* peak (285.3 eV) in Ni/Graphene than in almost pure graphene suggests a higher degree of wrinkling and folding within the graphene nanoplatelet after Ni nanoparticle deposition[29], suggesting a strong interaction between them, presumably that the Ni nanoparticles are favorably adsorbed on the hollow of the graphene hexagons, bridge of C-C bonds and are placed on top of C atoms[16], resulting in deformation of the graphene nanoplatelet. The less intense peak at 287.5 eV is due to $\sigma^*_{C\text{-}H}$ or aromatic hydroxyl $\sigma^*_{C\text{-}OH}$ or epoxyl $\sigma^*_{C\text{-}O\text{-}C}$ band, while the peak at 288.5 eV is dominated by carboxyl groups $\pi^*_{O\text{-}C=O}$. The most sharp and intense peaks at 291.7 and 292.7 eV are featured as a resolved double-peak via $\sigma^*_{C\text{-}C}$ resonance[21]. Among these localized features, when compared to those of graphene, the Ni/Graphene spectrum exhibits enhanced intensity between 287 - 290 eV due to additional carbon-oxygen functional groups (most likely the interface oxygen bridge between Ni and Graphene), and reduced intensity in the intensity-flipped double-peak σ* (291.7 and 292.7 eV) probably because of a significant charge transfer effect (more details to follow at the Ni 2p edge) and a weak polarization effect associated with a slightly higher degree of wrinkling and folding

for the graphene substrate. These spectroscopic changes suggest that the graphene framework was strongly interacted/functionalized with Ni nanoparticles via Ni-C and Ni-O-C (including nickel carbonate Ni-O-C=O) covalent bonding structures.

At the O 1s in Fig. 2c, compared to almost pure graphene (red line) and Ni (green line) and their linear combination, O 1s spectrum of Ni/Graphene (blue line) displays an overall enhanced π* and σ* intensity, strongly suggesting additional bonding/carbon-oxygen functional groups in Ni/Graphene via Ni-O-C bonding structure to anchor Ni nanoparticles onto the graphene substrate, which is consistent with the C K-edge result. The correlated peaks at 532.3 and 539.9 eV are the characteristics of carboxyl groups ($\pi^*_{O\text{-}C=O}$) and $\sigma^*_{C\text{-}O}$ band[21], respectively. Another pronounced peak in both Ni/Graphene and Ni at ~538 eV is attributed to the $\sigma^*_{O\text{-}Ni}$ band and it is absent in the almost pure graphene region.

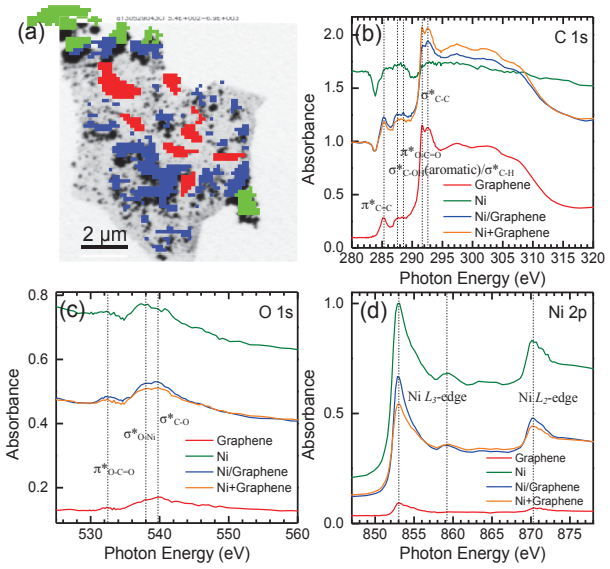

Fig. 2 STXM XANES spectra of a single Ni/Graphene nanoplatelet, (a) selected regions on the sample to exact XANES spectra by STXM stacks, red regions: almost pure graphene, green regions: almost pure metallic Ni particles off the nanoplatelet, and blue regions: Ni/Graphene; (b) C 1s, (c) O 1s, and (d) Ni 2p XANES spectra of the selected color coded regions in (a), a linear combination of the pure Ni and graphene spectra (i.e. 0.45*Ni + 1.0*Graphene, orange lines) is included to compare with Ni/Graphene. All vertical dashed lines in the spectra indicate the spectral regions of interest and are labelled with electronic structure assignments.

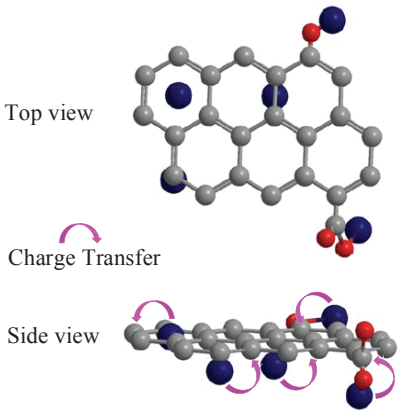

Fig. 3 Schematic configuration of Ni attachment upon graphene framework in Ni/Graphene. Ni atoms adsorb on the hollow of the graphene hexagons, bridge of C-C bonds, top of C atoms, and Ni attached to oxygen functional groups via Ni-O-C covalent bonding. The gray, red and blue balls represent C, O and Ni atoms, respectively. The purple curved arrows indicate charge transfer from Ni to graphene.

Fig. 2d presents the Ni 2p XANES spectra from the three regions. Two main peaks at ~853.0 eV and 870.1 eV are located at the same energies of the elemental Ni $2p_{3/2}$ (L_3-edge) and Ni $2p_{1/2}$ (L_2-edge) levels[39], respectively. In addition, there is no evident peak splitting in the Ni 2p peaks for both Ni and Ni/Graphene, indicating that the oxidation state for both is Ni(0). The Ni 2p edge jump of the Ni spectrum is about double of that of Ni/Graphene, suggesting the Ni thickness in the former is about twice of the latter, which is in good agreement with the spectrum fitting coefficients in Fig. 2. This also implies that Ni nanoparticles off the graphene nanoplatelet tend to aggregate significantly. Compared to Ni+Graphene (orange line), the Ni 2p spectrum of Ni/Graphene (blue line) shows significantly enhanced L_3 and L_2 edges (i.e. unoccupied states), suggesting a significant net charge transfer from Ni to graphene since the Ni(0) oxidation state was essentially reserved. This is considered as a result from covalent bonding of Ni-C and Ni-O-C, and the other striking observation of the charge transfer is that in the C 1s edge the $\sigma^*_{C\text{-}C}$ intensities (291.7 and 292.7 eV sharp features and other broad features from 295 to 310 eV) of graphene were significantly reduced, confirming the charge transferred to the graphene framework as XANES probes the UDOS at the carbon sites. The schematic configuration of Ni attachment upon graphene framework in Ni/Graphene is displayed in Fig. 3, showing the Ni adsorbed, functionalized sites, as well as the charge transfer from Ni to graphene. Although trace amount of oxygen was detected at both regions, it was most likely due to surface oxidation of the Ni(0) nanoparticles. Based on above information, the covalent interactions between Ni and graphene significantly help stabilize the nanostructure, which is expected to substantially extend the lifecycle of the host material for hydrogen uptake. Further hydrogen storage test of this material is underway.

In summary, STXM has been performed to obtain chemical mapping and XANES of Ni/Graphene nanocomposite. It has been found that Ni nanoparticles prepared from thermal reduction of nickel acetate deposit mainly on the graphene substrate with a small portion of the aggregated Ni particles attached to the edge of graphene nanoplatelet or depleted completely. The spatially resolved XANES at multiple elemental edges allowed to determine the Ni (0) state, and the local chemistry and electronic structure, revealing the anchoring of Ni(0) nanoparticles onto the graphene substrate via Ni-C and Ni-O-C covalent bonding. These results have advanced our understanding of the electronic and chemical structure of Ni/Graphene, and other similar TM/Graphene systems, and will help optimizing the tailoring of TM/Graphene host materials for hydrogen storage.

The Canadian Light Source is supported by the Natural Sciences and Engineering Research Council of Canada, the National Research Council Canada, the Canadian Institutes of Health Research, the Province of Saskatchewan, Western

Economic Diversification Canada, and the University of Saskatchewan.

[a] *Department of Mechanical Engineering, University of Saskatchewan, Saskatoon, SK, S7N 5A9, Canada.*
**E-mail: jerzy.szpunar@usask.ca*
[b] *Canadian Light Source Inc., Saskatoon, SK, S7N 2V3, Canada.*
**E-mail: jian.wang@lightsource.ca*

† Electronic Supplementary Information (ESI) available: [sample preparation and characterization by laborotory based techniques], See DOI: 10.1039/b000000x/

Notes and references

1. T. B. Johansson, *Renewable energy: sources for fuels and electricity*, Island Pr, 1993.
2. M. Hoel and S. Kverndokk, *Resource and Energy Economics*, 1996, **18**, 115-136.
3. G. W. Crabtree, M. S. Dresselhaus and M. V. Buchanan, *Physics Today*, 2004, **57**, 39.
4. C.-J. Winter and J. Nitsch, 1988.
5. T. Hua, R. Ahluwalia, J.-K. Peng, M. Kromer, S. Lasher, K. McKenney, K. Law and J. Sinha, *International Journal of Hydrogen Energy*, 2011, **36**, 3037-3049.
6. L. Schlapbach and A. Züttel, *Nature*, 2001, **414**, 353-358.
7. I. F. Silvera, *Reviews of Modern Physics*, 1980, **52**, 393.
8. D. P. Broom, in *Hydrogen Storage Materials*, Springer, 2011, pp. 117-139.
9. A. K. Geim and K. S. Novoselov, *Nat Mater*, 2007, **6**, 183-191.
10. H. L. Poh, F. Šaněk, Z. Sofer and M. Pumera, *Nanoscale*, 2012, **4**, 7006-7011.
11. S. Li, H.-m. Zhao and P. Jena, *Frontiers of Physics*, 2011, **6**, 204-208.
12. M. Pumera, *Energy & Environmental Science*, 2011, **4**, 668-674.
13. G. Sandrock, *Journal of Alloys and Compounds*, 1999, **293**, 877-888.
14. B. Vinayan, K. Sethupathi and S. Ramaprabhu, *Journal of Nanoscience and Nanotechnology*, 2012, **12**, 6608-6614.
15. I. Cabria, M. Isla, M. Lopez, J. Martınez, L. Molina, J. Alonso and C. O. Head, *Nanoclusters: A Bridge Across Disciplines*, 2010, **1**, 299.
16. Z. Ao and F. Peeters, *Physical Review B*, 2010, **81**, 205406.
17. G. K. Dimitrakakis, E. Tylianakis and G. E. Froudakis, *Nano letters*, 2008, **8**, 3166-3170.
18. V. Rigo, T. Martins, A. J. da Silva, A. Fazzio and R. Miwa, *Physical Review B*, 2009, **79**, 075435.
19. G. Wei, Y.-E. Miao, C. Zhang, Z. Yang, Z. Liu, W. W. Tjiu and T. Liu, *ACS Applied Materials & Interfaces*, 2013, **5**, 7584-7591.
20. I. S. Youn, D. Y. Kim, N. J. Singh, S. W. Park, J. Youn and K. S. Kim, *Journal of Chemical Theory and Computation*, 2011, **8**, 99-105.
21. Y. Cho, Y. C. Choi and K. S. Kim, *The Journal of Physical Chemistry C*, 2011, **115**, 6019-6023.
22. Y. Wang, C. X. Guo, X. Wang, C. Guan, H. Yang, K. Wang and C. M. Li, *Energy & Environmental Science*, 2011, **4**, 195-200.
23. L. Zheng, Z. Li, S. Bourdo, F. Watanabe, C. C. Ryerson and A. S. Biris, *Chemical Communications*, 2011, **47**, 1213-1215.
24. S.-Y. Lee and S.-J. Park, *Journal of nanoscience and nanotechnology*, 2013, **13**, 443-447.
25. J. Zhou, J. Wang, C. Sun, J. Maley, R. Sammynaiken, T. Sham and W. Pong, *Journal of Materials Chemistry*, 2011, **21**, 14622-14630.
26. J. Zhou, J. Wang, H. Liu, M. N. Banis, X. Sun and T.-K. Sham, *The Journal of Physical Chemistry Letters*, 2010, **1**, 1709-1713.
27. J. Zhou, J. Wang, Y. Hu, T. Regier, H. Wang, Y. Yang, Y. Cui and H. Dai, *Chem. Commun.*, 2013, **49**, 1765-1767.
28. J. Zhou, J. Wang, L. Zuin, T. Regier, Y. Hu, H. Wang, Y. Liang, J. Maley, R. Sammynaiken and H. Dai, *Physical Chemistry Chemical Physics*, 2012, **14**, 9578-9581.
29. J. Wang, J. Zhou, Y. Hu and T. Regier, *Energy & Environmental Science*, 2013.
30. G. Liu, Y. Wang, F. Qiu, L. Li, L. Jiao and H. Yuan, *Journal of Materials Chemistry*, 2012, **22**, 22542-22549.
31. M. Giovanni, H. L. Poh, A. Ambrosi, G. Zhao, Z. Sofer, F. Šaněk, B. Khezri, R. D. Webster and M. Pumera, *Nanoscale*, 2012, **4**, 5002-5008.
32. S. Mayavan, J.-B. Sim and S.-M. Choi, *Journal of Materials Chemistry*, 2012, **22**, 6953-6958.
33. V. Georgakilas, M. Otyepka, A. B. Bourlinos, V. Chandra, N. Kim, K. C. Kemp, P. Hobza, R. Zboril and K. S. Kim, *Chemical Reviews*, 2012, **112**, 6156-6214.
34. Y. Kim, J. Lee, M. S. Yeom, J. W. Shin, H. Kim, Y. Cui, J. W. Kysar, J. Hone, Y. Jung and S. Jeon, *Nature communications*, 2013, **4**.
35. C. Bao, L. Song, W. Xing, B. Yuan, C. A. Wilkie, J. Huang, Y. Guo and Y. Hu, *Journal of Materials Chemistry*, 2012, **22**, 6088-6096.
36. Y. Liang, Y. Li, H. Wang, J. Zhou, J. Wang, T. Regier and H. Dai, *Nature materials*, 2011, **10**, 780-786.
37. Z. Liu, K. Suenaga, P. J. Harris and S. Iijima, *Physical review letters*, 2009, **102**, 015501.
38. M. Akhukov, A. Fasolino, Y. Gornostyrev and M. Katsnelson, *Physical Review B*, 2012, **85**, 115407.
39. J. F. Moulder, J. Chastain and R. C. King, *Handbook of X-ray photoelectron spectroscopy: a reference book of standard spectra for identification and interpretation of XPS data*, Physical Electronics Eden Prairie, MN, 1995.